International Journal of Mechanical, Industrial and Aerospace Sciences
ISSN: 2517-9950
Vol:10, No:8, 2016

A Compact Quasi-Zero Stiffness Vibration Isolator Using Flexure-Based Spring Mechanisms Capable of Tunable Stiffness

Thanh-Phong Dao, Shyh-Chour Huang

***Abstract*—**This study presents a quasi-zero stiffness (QZS) vibration isolator using flexure-based spring mechanisms which afford both negative and positive stiffness elements, which enable self-adjustment. The QZS property of the isolator is achieved at the equilibrium position. A nonlinear mathematical model is then developed, based on the pre-compression of the flexure-based spring mechanisms. The dynamics are further analyzed using the Harmonic Balance method. The vibration attention efficiency is illustrated using displacement transmissibility, which is then compared with the corresponding linear isolator. The effects of parameters on performance are also investigated by numerical solutions. The flexure-based spring mechanisms are subsequently designed using the concept of compliant mechanisms, with evaluation by ANSYS software, and simulations of the QZS isolator.

***Keywords*—**Vibration isolator, quasi-zero stiffness, flexure-based spring mechanisms, compliant mechanism.

I. Introduction

PASSIVE linear isolator is able to effectively decrease vibration when its natural frequency is less than $\sqrt{2}$ times that of the excitation frequencies. Low stiffness is desired in order to enhance the bandwidth of the isolator, but this causes an undesired large deflection. To overcome this limitation, high static stiffness but with low dynamic stiffness has thus far been more suitable for passive vibration isolators. Ideally, the positive stiffness should be equal to the negative stiffness at an equilibrium position under a designed load, which results in the definition of an isolator with high static stiffness but low dynamic stiffness, called a QZS isolator.

Many QZS isolators have been studied in depth over the last two decades. Platus [1] suggested a 6-dof passive isolator using flexure beams as negative stiffness coupled with a coil spring, resulting in zero stiffness. Carrella et al. [2] used a vertical spring with oblique springs to construct a QZS isolator, and analyzed its statics. Gatti et al. [3] studied the dynamic behaviors of a 2-dof system for a QZS isolator via horizontal springs coupled with oblique springs. Huang et al. [4] used a Euler buckled beam as the negative stiffness corrector in order to improve the isolator, and investigated the stiffness and dynamic characteristics theoretically. In addition, QZS isolators can be designed in other ways. Zhou et al. [5] proposed horizontal cam–roller–spring mechanisms and vertical coil springs to cancel the stiffness of the spring for a QZS isolator. Xu et al. [6] proposed a vibration isolator combining a positive stiffness spring with a novel magnetic spring with negative stiffness in parallel to improve the performance of the isolator. Kovacic et al. [7], [8] studied the statics and dynamics of QZS stiffness. Robertson et al. [9] studied design parameters for a QZS magnetic spring for isolation. In the field of vehicle driver vibration isolators, negative springs were used to minimize fundamental frequencies of the isolator by Lee et al. [10]. Zhou and Liu [11] used a mechanical spring as a flexible beam, in parallel with a magnetic spring to produce tunable QZS stiffness for the isolator. Negative stiffness was examined by Ibrahim [12]. Le and Ahn [13] presented an experimental investigation of a QZS isolator with negative stiffness. In the field of flexure-based mechanisms, Kim et al. [14] presented an optimal design of a QZS isolator using flexures for a wide range of payloads. Recently, Meng et al. [15] analyzed QZS isolator with a disk spring as negative stiffness element.

Almost all existing QZS isolators focus on vibration attenuation. However, far too little attention has been paid to the use of compliant mechanisms to make flexure-based spring mechanisms for QZS vibration isolators: springs that are able to self-adjust their stiffness. Compared with conventional mechanisms, compliant mechanisms offer advantages such as non-friction, lubrication-free, easy to fabricate, allowing for monolithic manufacturing, and minimal maintenance [16]-[24].

This paper presents a QZS isolator for translational vibration based on the concept of compliant mechanisms. Using compliant mechanisms, flexure-based spring mechanisms are designed to provide both negative and positive stiffness. Compliant mechanisms possess advantages, such as being friction-free, lubrication-free, easy to fabricate, suitable for monolithic manufacturing, and requiring minimal maintenance. The QZS isolator presented in this paper can therefore be implemented in miniature space.

This study covers the statics and dynamics of this QZS isolator with flexure-based spring mechanisms. The non-dimensional stiffness of the isolator is then approximated by a polynomial function using a Taylor series expansion up to the order of 4 in order to analyze the dynamics of the system. The nonlinear equation of the motion of the isolator is solved

Shyh-Chour Huang is with the Department of Mechanical Engineering, National Kaohsiung University of Applied Sciences, 415 Chien-Kung Road, Kaohsiung 80778, Taiwan, ROC (corresponding author, phone.: (07)-3814526 ext 5313, fax: (07)-3831373, e-mail: shuang@cc.kuas.edu.tw).

Thanh-Phong Dao is with Division of Computational Mechatronics (DCME), Institute for Computational Science (INCOS), Ton Duc Thang University, Ho Chi Minh City, Vietnam and with Faculty of Electrical & Electronics Engineering, Ton Duc Thang University, Ho Chi Minh City, Vietnam.

using the Harmonic Balance method, which determines the relationships among the displacement amplitude, excitation amplitude, and frequency. Moreover, the performance of the isolator is evaluated using displacement transmissibility, which is compared with a corresponding linear isolator with a QZS isolator that only has positive stiffness.

II. Description of the Model

The model is based on the design concept initially suggested by Platus [1], who used horizontal flexure beams to achieve a negative stiffness, and a vertical coil spring representing a positive stiffness, as given in Fig. 1 (a). Here, a schematic diagram of a QZS isolator with flexure-based spring mechanisms (FBSM) is developed without a coil spring, as shown in Fig. 1 (b). A physical prototype model of a QZS isolator with FBSMs at the static equilibrium position is shown in Fig. 1 (c). An exploded model of the isolator is presented in Fig. 2. The entire system is fixed on a platform (1), which is excited by an exciter. Two vertical springs with positive stiffness k_p (7) are coupled with two horizontal springs with negative stiffness k_n (6) and (10) through the top inner ring (9) and bottom inner ring (14). The vertical springs provide positive stiffness and adjust displacement by a vertical adjusting screw (15). The vertical adjusting screw is connected to the base (2) which is fixed to the platform. The horizontal springs provide a negative stiffness. The horizontal springs are connected with left sliders (4) and (12), which can move on rays (3) and (13). The displacement of the horizontal springs can be adjusted by adjusting screws (5) and (11). An isolated object W has weight m (8). The springs are designed with FBSMs in order to enable application within a miniature space.

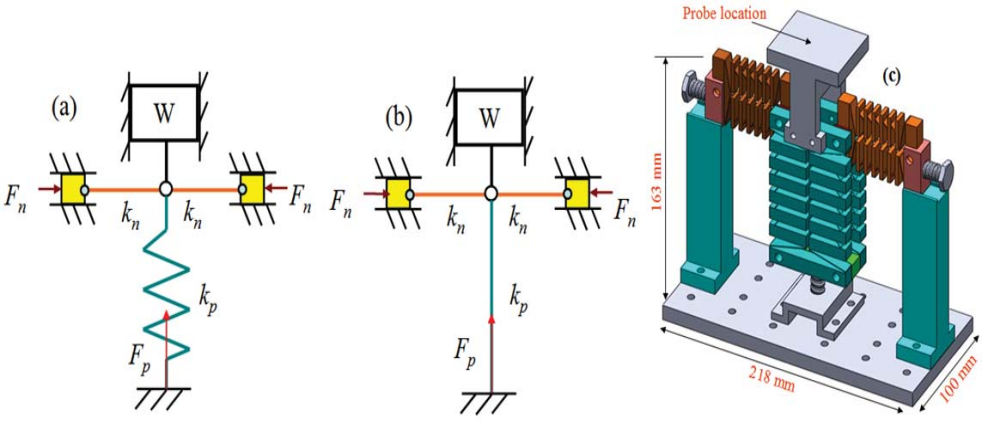

Fig. 1 Schematic diagram of QZS isolator: (a) A traditional isolator with two horizontal flexure beams [1], (b) QZS isolator with FBSM, (c) physical prototype model

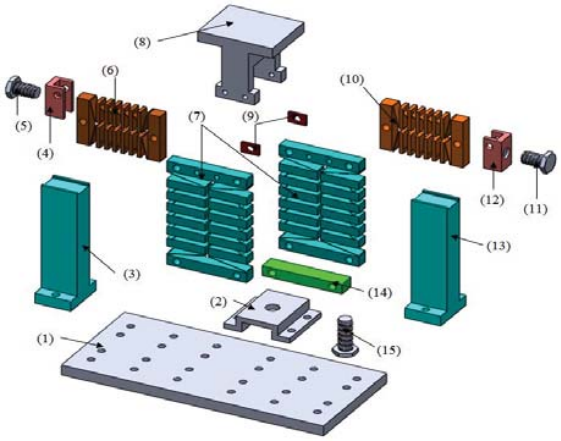

Fig. 2 Exploded model of isolator: (1) platform, (2) base, (3) left ray, (4) left slider, (5) left adjusting screw, (6) left horizontal spring with negative stiffness kn, (7) vertical springs with positive stiffness kp, (8) weight load, (9) top inner ring, (10) right horizontal spring with negative stiffness kn, (11) right adjusting screw, (12) right slider, (13) right ray, (14) bottom inner ring, (15) vertical adjusting screw

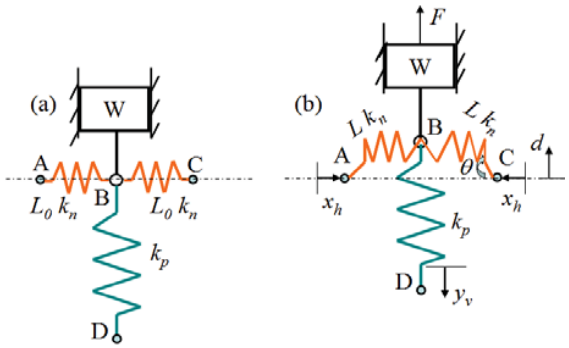

Fig. 3 Schematic diagram: (a) At equilibrium position, (b) deviation from equilibrium position by a displacement *d*

III. Static Analysis

The isolator with FBSMs is initially in a static equilibrium position, as shown in Fig. 3 (a). At the static equilibrium position, points A, B and C are the collinear points. In order to achieve the static equilibrium position, adjustments must be made by screws (5), (11) and (15). Unlike previous studies, the adjusters are considered in this study. Therefore, at equilibrium

position, the vertical springs and the horizontal springs are compressed by deflection $\delta_y = \Delta y - y_v$ (δv = mg/kp) and $\delta_x = \Delta x - x_h$, respectively, where mg is the payload, yv is the vertical adjustment, xh is horizontal adjustment, and Δy and Δx are the deflections of the vertical and horizontal springs, respectively. When the negative stiffness of the horizontal springs is equal to the positive stiffness of the vertical springs at the equilibrium position, the isolator with FBSMs will achieve the QZS property, hence, the so-called zero-stiffness condition.

When a force *F* is applied, it causes a vertical displacement d from the static equilibrium position, as shown in Fig. 3 (b). Therefore, the relationship between the applied force and displacement can be studied, and further discussion of the stiffness of the isolator is provided. Note that the magnitude of the restoring force and the applied force are balanced, but in opposite directions. The static equilibrium equation of the system can be given by:

$$F(d) = mg - F_p - 2F_h \sin\theta \tag{1}$$

where vertical spring force is $F_p = k_p\left[(\Delta y - y_v) - (d - y_v)\right]$, and horizontal spring force is $F_n = k_n\left[(\Delta x - x_h) - (L - L_0)\right]$, $L = \sqrt{(L_0 - x_h)^2 + d^2}$, $\sin\theta = d/L$. L is the stretched length of the horizontal springs and L_0 is the initial length of the horizontal springs.

The vertical spring is compressed by a deflection $\delta_y = \Delta_y - y_v$ and the horizontal spring is compressed by a deflection $\delta_x = \Delta x - x_h$. Therefore, the applied force *F* related to the displacement *d* can be determined by:

$$F(d) = k_p(d - y_v) - 2k_n d\left(\frac{\delta_x + L_0}{\sqrt{(L_0 - x_h)^2 + d^2}} - 1\right) \tag{2}$$

Take (2) divided by k_pL_0, and the non-dimensional force yields:

$$\hat{F}(\hat{d}) = (\hat{d} - \hat{y}_v) - 2\alpha\hat{d}\left(\frac{\hat{\delta}_x + 1}{\sqrt{(1 - \hat{x}_h)^2 + \hat{d}^2}} - 1\right) \tag{3}$$

where $\hat{F} = F/k_pL_0$, $\alpha = k_n/k_p$, and the geometric ratio is $\hat{y}_v = y_v/L_0$, $\hat{\delta}_x = \delta_x/L_0$, $\hat{x}_h = x_h/L_0$, and $\hat{d} = d/L_0$.

Take the derivative of (3) with respect to non-dimensional displacement, and the non-dimensional stiffness of the system can be achieved as:

$$\hat{k} = 1 - 2\alpha\left(\frac{(\hat{\delta}_x + 1)(1 - \hat{x}_h)^2}{\left[(1 - \hat{x}_h)^2 + \hat{d}^2\right]^{3/2}} - 1\right) \tag{4}$$

There is a unique condition between the parameters α and δ_x, which results in the zero stiffness characteristics at the static equilibrium position. This condition is obtained by setting $\hat{k}(\hat{d} = 0) = 0$. And to make the stiffness equation more general, the horizontal adjustment sets $\hat{x} = 1/2$. Thus, the QZS condition is yielded as:

$$\hat{\delta}_{QZS} = \hat{\delta}_x = \frac{1}{4\alpha} - \frac{1}{2} \tag{5}$$

Substituting (5) into (3) and (4), the force-displacement relationship and the QZS stiffness of the QZS isolator can be given respectively by:

$$\hat{F}(\hat{d}) = (\hat{d} - \hat{y}_v) - 2\hat{d}\left(\frac{1}{4\hat{\delta}_{QZS} + 2}\right)\left(\frac{\hat{\delta}_{QZS} + 1}{\sqrt{(1 - \hat{x}_h)^2 + \hat{d}^2}} - 1\right) \tag{6}$$

$$\hat{k}_{QZS} = 1 - 2\left(\frac{1}{4\hat{\delta}_{QZS} + 2}\right)\left(\frac{(\hat{\delta}_{QZS} + 1)(1 - \hat{x}_h)^2}{\left[(1 - \hat{x}_h)^2 + \hat{d}^2\right]^{3/2}} - 1\right) \tag{7}$$

For $\hat{y}_v = 0$, $\hat{x}_h = 1/2$, Fig. 4 shows the non-dimensional force-displacement characteristic for different values of $\hat{\delta}_x$ ($\hat{\delta}_x = -0.4$, $\hat{\delta}_x = -0.25$, and $\hat{\delta}_x = 0.2$). A smaller negative value of $\hat{\delta}_x$ leads to a slightly positive stiffness. In contrast, a larger compressed deflection in the positive direction leads to a slightly negative stiffness near the equilibrium position.

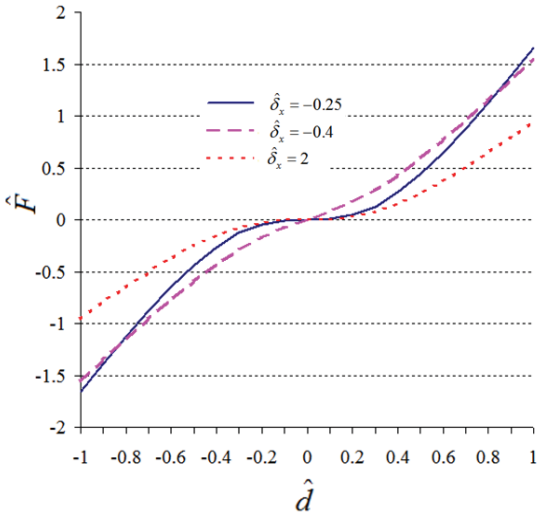

Fig. 4 Force-displacement curves with different $\hat{\delta}_x$

Fig. 5 compares the non-dimensional stiffness curves for $\hat{\delta}_x = -0.4$, $\hat{\delta}_x = -0.25$, and $\hat{\delta}_x = 0.2$. Although all three curves achieve zero stiffness, a smaller negative value of $\hat{\delta}_x$ has a

larger average stiffness for a given region near the equilibrium position. Conversely, $\hat{\delta}_x$ towards a positive value, such as $\hat{\delta}_x = 0.2$, $\hat{\delta}_x$ has a smaller average stiffness.

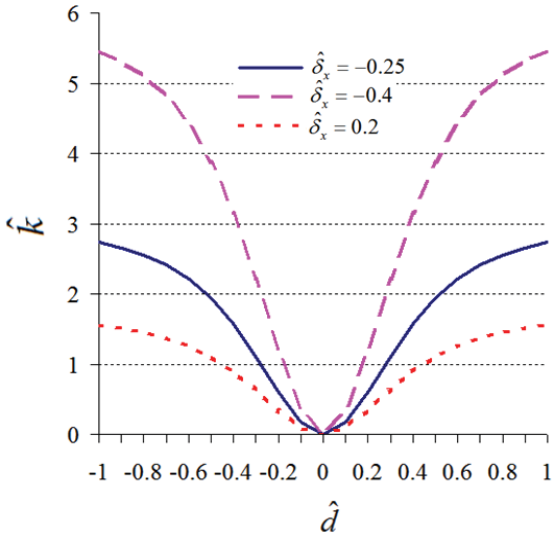

Fig. 5 Stiffness curves for different $\hat{\delta}_x$

IV. Dynamic Analysis

QZS is presented in this paper to suppress vertical vibrations with a high-static-low-dynamic stiffness when the base is excited causing vibration, which is transmitted to the isolating system. The vibration level of the isolated object W depends on the dynamic stiffness of the vibration isolator. The isolator is supported by a frame whose displacement is represented by z. The frame is excited via a sinusoidal displacement z with magnitude Z and frequency w to describe external disturbance, as depicted in Fig. 6. The damping effect on the isolator is illustrated using a viscous damper added with the vertical spring in parallel so that the equation of the motion for the vibration isolator system under harmonic excitation accounts for dissipative terms.

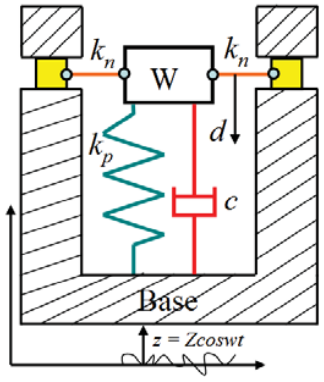

Fig. 6 Schematic diagram of dynamic model

The governing equation of the dynamics of the isolator is achieved using Lagrange's formulation. First, the kinetic energy T and potential energy V of the isolator are as:

$$T = \frac{1}{2}m\left(\dot{d} + \dot{z}\right) \text{ and } V = \frac{1}{2}kd^2 \tag{8}$$

where m is the mass of the isolated load W, and k is the stiffness of the isolator system, as derived in (4).

The dissipation function C can be described as:

$$C = \frac{1}{2}c\dot{d}^2 \tag{9}$$

where c is the damping coefficient of the damper. The dynamic equation of the isolator is derived by combining (8) and (9).

The Lagrange L_a is formed by taking the difference of the scalar quantities of kinematic energy T and potential energy V of the system, $L_a = T - V$.

Using Lagrange's formulation, the equation of the motion for the QZS system is expressed in non-dimensional form as:

$$\hat{d}'' + 2\xi\hat{d}' + \hat{k}_{QZS}\hat{d} = \hat{Z}\Omega^2\cos\Omega\tau \tag{10}$$

by introducing the non-dimensional parameters as:

$$\begin{cases} \xi = \dfrac{c}{2mw_0}, \hat{Z} = \dfrac{Z}{L_0}, \Omega = \dfrac{w}{w_0}, \hat{k}_{QZS} = \dfrac{k}{k_p}, \\ \tau = w_0 t, \hat{d}'' = \dfrac{\ddot{\hat{d}}}{w_0^2}, \hat{d}' = \dfrac{\dot{\hat{d}}}{w_0}, \hat{d} = \dfrac{d}{L_0} \end{cases} \tag{11}$$

where $w_0 = \sqrt{k_p / m}$ is the un-damped natural frequency of the system without negative stiffness.

Recalling (4), in order to simplify the subsequent dynamic analysis, the relationship between stiffness and displacement is approximated by a polynomial using a Taylor series expansion up to an order of 4 expanded about the equilibrium position d = 0 and for x_h =0, defined by:

$$\hat{k}_{QZS} = \hat{k}_{QZS}(0) + \sum_{n=1}^{4} \frac{\hat{k}_{QZS}^{(n)}(0)}{n!} \tag{12}$$

where

$$\begin{cases} \hat{k}_{QZS}(0) = 1 - 2\alpha\hat{\delta}_{QZS} \\ \hat{k}_{QZS}^{(1)}(0) = 0 \\ \hat{k}_{QZS}^{(2)}(0) = 6\alpha\left(\hat{\delta}_{QZS} + 1\right) \\ \hat{k}_{QZS}^{(3)}(0) = 0 \\ \hat{k}_{QZS}^{(4)}(0) = -54\alpha\left(\hat{\delta}_{QZS} + 1\right) \end{cases} \tag{13}$$

The dynamic equation of motion of the isolator is derived as:

$$\hat{d}'' + 2\xi\hat{d}' + 1 - 2\alpha\hat{\delta}_{QZS} + 3\alpha\left(\hat{\delta}_{QZS} + 1\right)\hat{d}^2 - \frac{9}{4}\alpha\left(\hat{\delta}_{QZS} + 1\right)\hat{d}^4 = \hat{Z}\Omega^2\cos\Omega\tau \tag{14}$$

where the prime (.)′ represents differentiation with respect to τ.

The Harmonic Balance method is a useful method that is not restricted to weak nonlinear problems, and has high accuracy. This method is adopted here to solve (14) and find the first approximation of the primary response.

Introducing a phase in excitation terms, (14) can be written as:

$$\hat{d}'' + 2\xi\hat{d}' + 1 - 2\alpha\hat{\delta}_{QZS} + 3\alpha\left(\hat{\delta}_{QZS} + 1\right)\hat{d}^2 - \frac{9}{4}\alpha\left(\hat{\delta}_{QZS} + 1\right)\hat{d}^4 = \hat{Z}\Omega^2\cos\left(\Omega\tau + \phi\right) \tag{15}$$

Assuming that the response solution of $\hat{d}$ is:

$$\hat{d} = \hat{D}\cos\left(\Omega\tau\right) \tag{16}$$

where $\hat{D} = D/L_0$.

Substituting (16) into (15) results in:

$$\begin{aligned} &-\hat{D}\Omega^2\cos\Omega\tau - 2\xi\hat{D}\Omega\sin\Omega\tau \\ &+3\alpha\left(\hat{\delta}_{QZS} + 1\right)\hat{D}^2\cos^2\Omega\tau \\ &-\frac{9}{4}\alpha\left(\hat{\delta}_{QZS} + 1\right)\hat{D}^4\cos^4\Omega\tau \\ &= \hat{Z}\Omega^2\cos\phi\cos\Omega\tau - \hat{Z}\Omega^2\sin\phi\sin\Omega\tau \end{aligned} \tag{17}$$

Neglecting the high order harmonic term, the coefficients of the same sines and cosines of (17) must be equal. This leads to:

$$-\hat{D}\Omega = \hat{Z}\Omega^2\cos\phi \tag{18a}$$

$$2\xi\hat{D}\Omega = \hat{Z}\Omega^2\sin\phi \tag{18b}$$

Squaring and adding (16a) and (16b) results in:

$$\left(\hat{D}\Omega\right)^2 + \left(2\xi\hat{D}\Omega\right)^2 = \left(\hat{Z}\Omega^2\right)^2 \tag{19}$$

Solving the above quadratic equation for Ω^2 yields:

$$\Omega = \frac{\hat{D}}{\hat{Z}}\sqrt{2\xi + 1} \tag{20}$$

The displacement transmissibility is defined as the ratio of the amplitudes between the absolute motion of the isolated object W and the base. The relative motion $\hat{d}$ is defined as $\hat{d} = d - z$, where d is the absolute vertical motion of the isolated object, and z is the excitation from the base. Thus, the amplitude of the absolute motion is $\hat{D} + \hat{Z}$. The displacement transmissibility is calculated as:

$$\begin{aligned} T &= \frac{\left\|\hat{D} + \hat{Z}\right\|}{\hat{Z}} = \frac{\sqrt{\left(\hat{D}^2 + \hat{Z}^2 + 2\hat{D}\hat{Z}\cos\phi\right)}}{\hat{Z}} \\ &= \frac{\sqrt{\left(\hat{D}^2 + \hat{Z}^2 - \frac{2\hat{D}^2}{\Omega}\right)}}{\hat{Z}} \\ &= \frac{\sqrt{\left(\hat{D}^2 + \hat{Z}^2 - 2\hat{Z}\hat{D}\sqrt{2\xi + 1}\right)}}{\hat{Z}} \end{aligned} \tag{21}$$

Equation (21) can written in the form of decibel as:

$$\begin{aligned} T &= 20\log_{10}\left(\sqrt{\left(\hat{D}^2 + \hat{Z}^2 - \frac{2\hat{D}^2}{\Omega}\right)\Big/\hat{Z}^2}\right) \\ &= 20\log_{10}\left(\sqrt{\left(\hat{D}^2 + \hat{Z}^2 - 2\hat{Z}\hat{D}\sqrt{2\xi + 1}\right)\Big/\hat{Z}^2}\right) \end{aligned} \tag{22}$$

V. Responses and Isolation Performance

A. Displacement-Time Response

The numerical simulation of displacement with respect to time is realized through approximately dynamic equation (10), as shown in Fig. 7. The input signal is consinusoid with amplitude $\hat{z}$ of 10, the excitation w = 1.5 rad/s and the phase ϕ of zero. Equation (10) is solved by using the Ode45 package in MATLAB. The physical parameters are used in the numerical simulation, given as follows: α = 1, ξ = 0.03, m = 5 kg, and k_p = 1.6 N/mm.

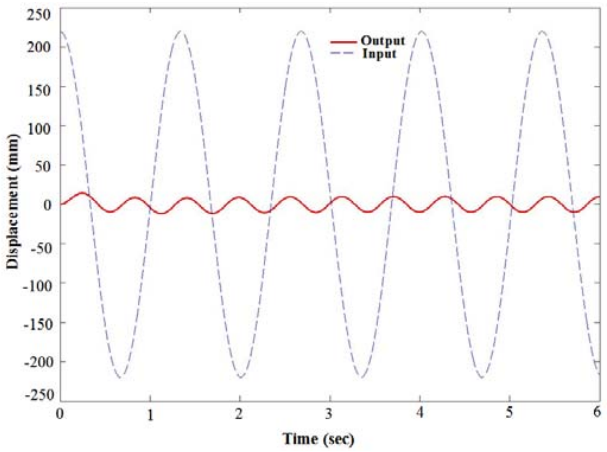

Fig. 7 Displacement response with respect to time history

B. Effect of Damping Ratio on Transmissibility

Fig. 8 shows the displacement transmissibility with respect to different damping ratios. The input displacement is $\hat{z}$ of 10, and Ω is in the range from 0 to 10. The peak of the transmissibility is the highest with respect to $\xi = 0$. When the

damping ratio increases, the peak value decreases. All curves are gradually oriented to the right.

C. Effect of Input Displacement on Transmissibility

The effect of the input displacement on the isolation range is given in Fig. 9. When the input displacement increases, the displacement transmissibility decreases.

D. Effect of Different Damping Ratios on the Natural Frequency

Fig. 10 shows the effect of different damping ratios on the natural frequency of the system. It is assumed that the ratio $\hat{D}/\hat{Z}$ remains constant while the damping ratio is a design variable. For example, in Fig. 10, the natural frequency is smallest with respect to $\xi = 0.2$, and the natural frequency is highest corresponding to $\xi = 0.14$. Thus, the natural frequency increases with an increased damping ratio.

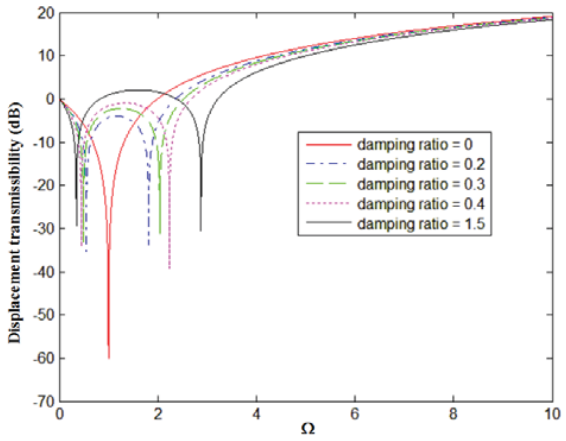

Fig. 8 Effect of damping ratio on displacement transmissibility

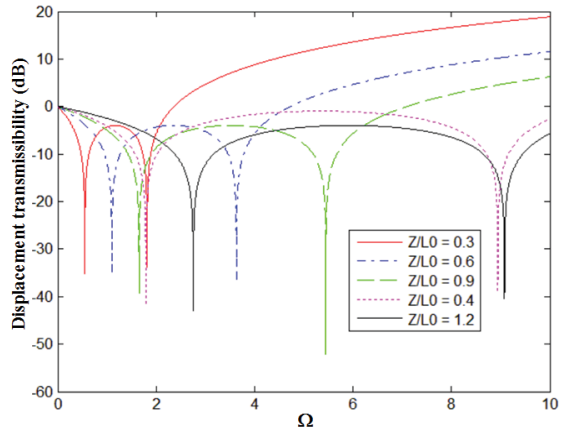

Fig. 9 Effect of input displacement on transmissibility

E. Comparison with a Linear Vibration Isolator

Fig. 11 shows a comparison between the presented QZS isolator and a linear system with respect to $\xi = 0.05$. It can be observed that the effective frequency of the isolator is smaller than that of the linear system, and the peak transmissibility of the isolator is less than that of the linear system. Another important observation is that the transmissibility of the isolator is lower than that of the linear isolator in the low frequency range. In terms of low frequency vibration isolators, the QZS vibration isolator system is superior to a linear system.

VI. Analysis of the Isolator

A. Analysis of Springs

As seen in Fig. 12, each vertical FBSM and each horizontal FBSM includes multiple cell structures combined in series. Fig. 13 gives a 2-D view of the cell structure. Each vertical and horizontal planar spring has six cells. Each cell consists of multiple flexure hinges connected with rigid links. The top and bottom of each planar spring is also connected with flexure hinges. Each flexure hinge has a rectangular cross section. The rectangular cross-section flexure hinge is chosen because its large deflection results in a reduced stiffness of overall structures. Each cell is placed in symmetry. For the vertical spring, each flexure hinge has an in-plane thickness t_1 and an out-plane thickness w_1. For the horizontal spring, each flexure hinge has an in-plane thickness t_2 and an out-plane thickness w_2. Table I presents the design parameters of the isolator.

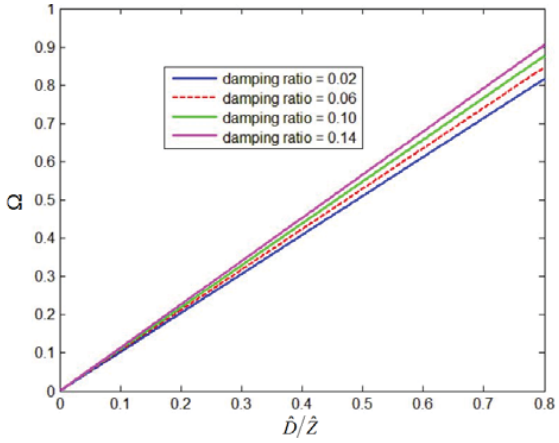

Fig. 10 Effect of damping ratio on the natural frequency

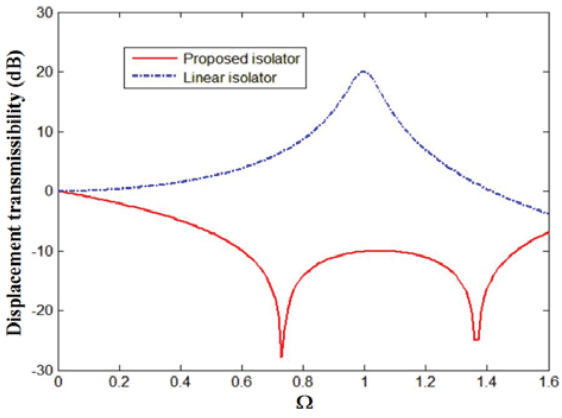

Fig. 11 Comparison between the presented isolator and a linear isolator

TABLE I
DESIGN PARAMETERS OF THE ISOLATOR

Parameters	Value	Unit
t_1	0.4	mm
t_2	0.4	mm
b_1	8	mm
b_2	3	mm
$w_1 = w_2$	10	mm
h_1	4.39	mm
h_2	4.39	mm
kn	15.5	N/mm
kp	4.5	N/mm

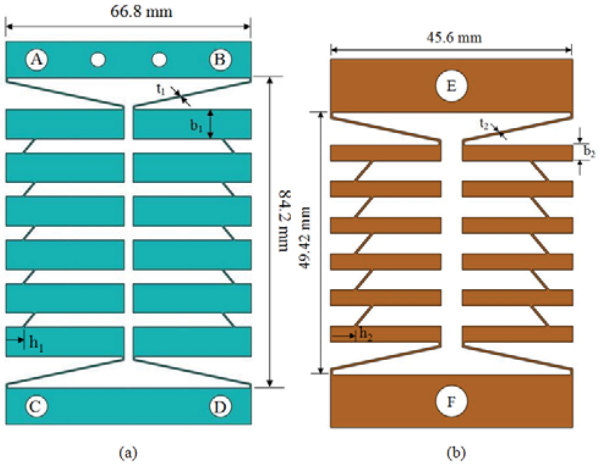

Fig. 12 (a) Vertical spring (84.2 mm × 66.8 mm × 10 mm), (b) horizontal spring (49.42 mm × 45.60 mm × 10 mm)

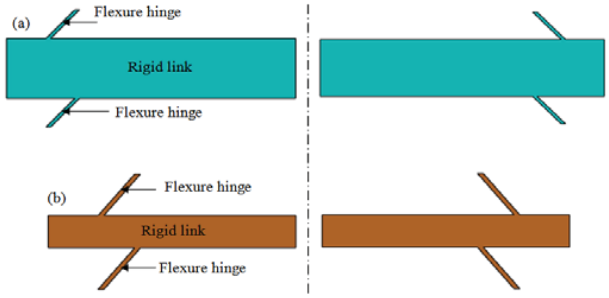

Fig. 13 2-D view of cell structure of: (a) vertical spring and (b) oblique spring

The stiffness of the isolator is dependent on the flexure hinges. Each flexure hinge is subjected to a bending load F; therefore, the deflection of the flexure hinges relies on them in-plane thickness and the out-plane thickness. This is expressed by:

$$\delta = \frac{FL^3}{3EI} \tag{23}$$

Thus, the stiffness of each flexure hinge is calculated as:

$$k = \frac{3Ewt^3}{4} \tag{24}$$

where, k is the stiffness of each flexure hinge, F is the bending load, E is Young's modulus of material, I is the sectional moment of inertia, w is the out of plane thickness of the flexure hinge, and t is the in-plane thickness of the flexure hinge.

From the above discussion, if a varying stiffness of the isolator is required, the out of plane thickness w of the flexure hinge or the in-plane thickness t of the flexure hinge must also be changed. A new stiffness of the isolator can be found by adjusting w or t for each spring in:

$$\frac{k_2}{k_1} = \frac{w_{22}t_{22}^3}{w_{11}t_{11}^3} \tag{25}$$

where, k is the stiffness and subscripts 1 and 2 indicate the original and new parameters, respectively. To achieve a new specific stiffness k_2, the value of t_{22} or w_{22} must be changed accordingly so that the right side of (25) is equal to the left side. Calculation, for instance, of k_p, k_{p2} is increased to 2.5 N/mm, while k_{p1} = 1.6 N/mm and w_{11} = 10 mm; then w_{22} should be adjusted to 15.625 mm if t_{22} is still unchanged. By adjusting the thickness, a new stiffness can be easily designed without changing the shape of the cell structure.

Another condition for adjusting the stiffness of the isolator is given by:

$$\frac{k_2}{k_1} = \frac{h_{22}}{h_{11}} \tag{26}$$

In (26), each cell of the springs is considered as a lever type amplification mechanism, in that its amplification ratio depends on the distance h from the end of the lever to a point located on the flexure hinge. Therefore, this study has discovered that only a change in the distance results in an adjustment in the stiffness k. The virtual prototype of two horizontal springs and two vertical springs are created. 65 Mn spring steel is chosen as the material for the springs because it is affordable and has high sensitivity, low elastic lag, and fatigue resistance. It also has a Young's modulus of 206000 MPa, yield strength of 784 MPa, a Poisson's ratio of 0.28 and density of 7850 kg/m^3.

Each horizontal FBSM weighs 130 g, while each vertical spring weighs 342 g. A static finite element analysis using ANSYS 13 is conducted to determine the stiffness of the springs. The automatic method is applied for meshing both springs. They are then refined to achieve a good meshing quality according to the Skewness criterion in ANSYS. The force-to-displacement curves of the horizontal and vertical springs are obtained to measure the stiffness, as shown in Figs. 14 (a) and (b), respectively. The average stiffness of each horizontal spring is 14.2871 N/mm, while the average stiffness of each vertical spring is 3.2164 N/mm. Both values are slightly lower than those desired, given in Table I (4.5 N/mm and 15.5 N/mm). The maximum displacement of the horizontal spring is Δ = 1.3999 mm when a load of 20 N is located at the top of the horizontal spring, as shown in Fig. 15 (a). The maximum displacement of the vertical spring is Δ = 6.2179 mm when a

load of 20 N is located at the top of the vertical spring, as shown in Fig. 15 (b).

Fig. 16 (a) illustrates the stress distribution of the horizontal spring versus the different displacements; the maximum stress is 359.23 MPa when the load is 20 N. Fig. 16 (b) illustrates the stress distribution of the vertical spring versus the different displacements; the maximum stress is 654.5 MPa when the load is 20 N. Both stresses are much smaller than the yield strength of 65 Mn spring steel (784 MPa). After analysis by FEA, the results revealed that the planar springs have linear characteristics similar to a coil spring. Therefore, the planar springs are adopted for the isolator. They are also applicable in situations that require more compact spaces. The number of components and complex assembly are reduced with the use of planar springs.

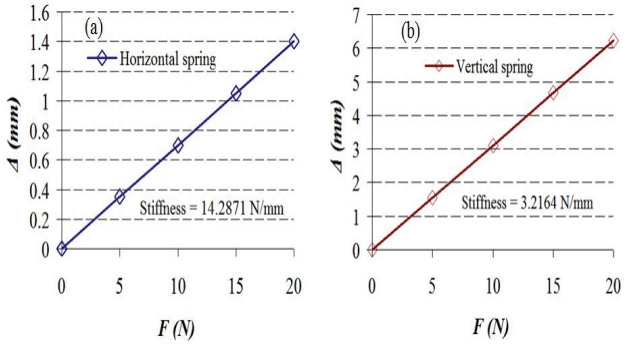

Fig. 14 Diagram of force-displacement curve: (a) horizontal spring, (b) vertical spring

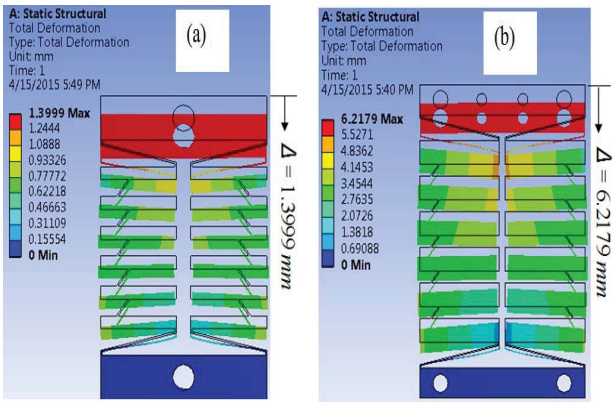

Fig. 15 Deformation of: (a) horizontal spring, (b) vertical spring

B. Static Analysis of the Isolator

For the mass m of the isolated load W of 0.25 kg, with other parameters retained as in Table I, for example, a static finite element analysis in ANSYS 13 is performed to illustrate the force-to-displacement curve of the isolator. A fixed boundary condition is at the bottom of the supporting platform. An applied force *F* is applied to the top plate of the load W. An automatic meshing is applied for the springs. A static finite element analysis using ANSYS 13 is conducted to determine the stiffness of the spring. The automatic method is applied for meshing both springs. They are then refined to achieve a good meshing quality according to the Skewness criterion in ANSYS. The force-to-displacement curve of the isolator is given in Fig. 17. The average stiffness of the isolator is 9.9265 N/mm.

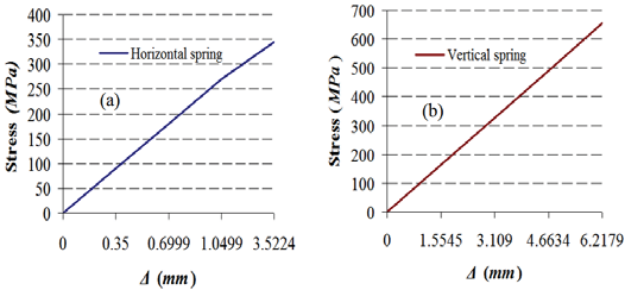

Fig. 16 Stress-displacement curve of: (a) horizontal spring, (b) vertical spring

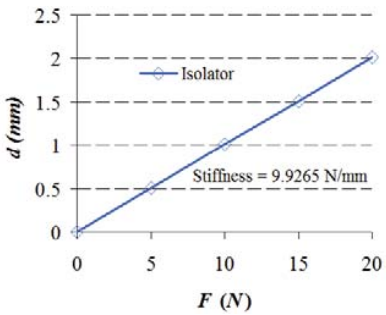

Fig. 17 Force-to-displacement curve of the isolator

C. Modal Analysis

ANSYS Modal module is used to execute the modal analysis. The boundary conditions of the isolator are fixed only at the bottom plate, but are free elsewhere. Six fundamental natural frequencies of the isolator are shown in Table II. The 1st, 2nd and 3rd modes are a linear mode of the load W along the z-axis at 12.410 Hz, 15.311Hz and 16.421Hz, respectively, as shown in Fig. 18 (a). The 4th mode is an up-down mode of the load W in the y-axis at 29.504 Hz, as shown in Fig. 18 (b). The 5th mode is a rolling mode of the load W around the z-axis at 30.055 Hz, as described in Fig. 18 (c). The 6th mode is a rolling mode of the load W around the x-axis at 36.856 Hz, as illustrated in Fig. 18 (d). The combination of a sufficient number of modes can build up a general motion of the isolator.

TABLE II
SIX FUNDAMENTAL NATURAL FREQUENCIES OF THE ISOLATOR

Modes	1	2	3	4	5	6
Natural frequencies (Hz)	12.410	15.311	16.421	29.504	30.055	36.856

D. Response Analysis

The compact dimensions of the isolator are 218 mm × 163 mm × 100 mm. The probe location of the estimated response is at the center of the isolated load W. The effects of various damping ratios ξ on the output displacement are considered, as shown in Fig. 19. Modal-based Harmonic module in ANSYS

with full method is used to describe the displacement response of the isolated load W. The peak response will correspond with the displacement response of the isolated load W. The value of ξ varies, such as 0 and 0.02. Beta damping is chosen as 0.07. The frequency range is from 0 Hz to 15 Hz. The input displacement is excited at the bottom. The peak of transmissibility with the damping ratio of 0.02 is always much less than that with a ξ of zero.

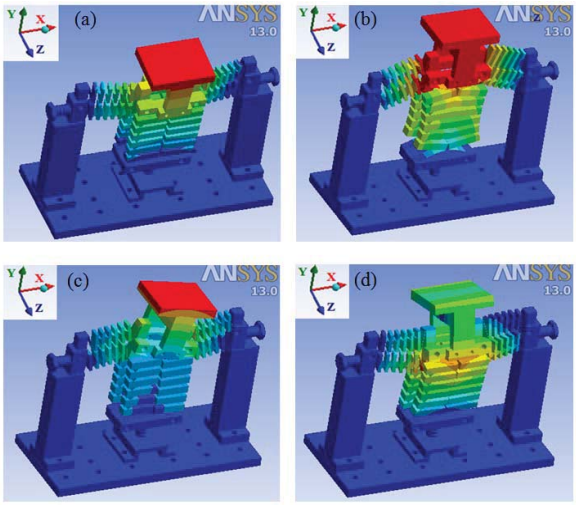

Fig. 18 Shape models: (a) The 1st, 2nd, and 3rd modes, (b) The 4th model, (c) The 5th mode, (d) The 6th mode

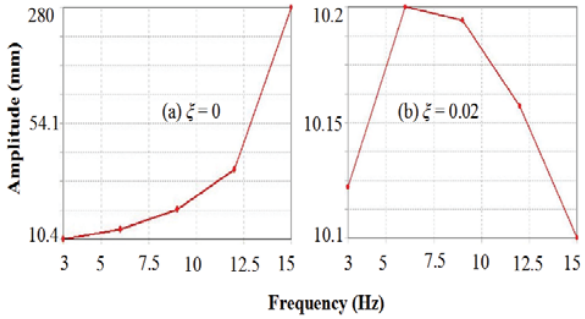

Fig. 19 Effect diagram of damping ratio on the output displacement: (a) $\xi = 0$, (b) $\xi = 0.02$

VII. Conclusion

This paper presented a QZS isolator for vertical vibration. FBSM were presented to provide negative and positive stiffness for the isolator using the concept of compliant mechanism. The stiffness of the springs can be redesigned to obtain a desired stiffness for various load weights. The isolator was easily assembled, and is very compact.

Static analysis was carried out to obtain the non-dimensional force and non-dimensional stiffness of the system. Furthermore, the dynamics of the system were also investigated using theoretical analysis. The nonlinear equations of the system were solved using the Harmonic Balance method. The efficiency of the isolator was evaluated by investigating the displacement transmissibility. It was found that the transmissibility of the QZS isolator is lower than that of current linear systems.

The static analysis of the springs was conducted using ANSYS software. The simulation of the QZS isolator was carried out to investigate the stiffness and performance. The results indicated that the stiffness of the springs is changed as little as possible and the QZS isolator is effective for compact spaces.

Future work will focus on constructing a prototype of the QZS isolator, and carrying out experimental investigations to confirm its effectiveness.

Acknowledgments

The authors acknowledge and thank the Ministry of Science and Technology of the Republic of China for their financial support of this study under Contract Number MOST 104-2221-E-151-010.

References

[1] D. Platus, "Negative-stiffness-mechanism vibration isolation systems," Proceedings of the SPIE's International Symposium on Vibration control in Microelectronics, Optics and Metrology, 1991.
[2] A. Carrella, M. J. Brennan, T. P. Waters, "Static analysis of a passive vibration isolator with quasi-zero-stiffness characteristic," Journal of Sound and Vibration, vol. 301, no. 3-5, pp. 678–689, 2007.
[3] G. Gatti, I. Kovacic, M. J. Brennan, "On the response of a harmonically excited two degree-of-freedom system consisting of a linear and a nonlinear quasi-zero stiffness oscillator," Journal of Sound and Vibration, vol. 329, pp. 1823–1835, 2010.
[4] X. C. Huang, X. T. Liu, J.Y. Sun, Z. Y. Zhang, "Vibration isolation characteristics of a nonlinear isolator using Euler buckled beam as negative stiffness corrector: A theoretical and experimental study, "Journal of Sound and Vibration, vol. 333, pp. 1132–1148, 2014.
[5] J. X. Zhou, X. L. Wang, D.L. Xu, S. Bishop, "Nonlinear dynamic characteristics of a quasi-zero stiffness vibration isolator with cam–roller–spring mechanisms," Journal of Sound and Vibration, vol. 346, pp. 53–69, 2015.
[6] D. Xu, Q. Yu, J. Zhou, S.R. Bishop, "Theoretical and experimental analyses of a nonlinear magnetic vibration isolator with quasi-zero-stiffness characteristic," Journal of Sound and Vibration, vol. 332, No.14, pp. 3377–3389, 2013.
[7] I. Kovacic, M. J. Brennan, T. P. Waters, "A study of a nonlinear vibration isolator with a quasi-zero stiffness characteristic," Journal of Sound and Vibration, vol. 315, pp. 700–711, 2008.
[8] I. Kovacic, M. J. Brennan, B. Lineton, "Effect of a static force on the dynamic behaviour of a harmonically excited quasi-zero stiffness system," Journal of Sound and Vibration, vol. 325, pp. 870–883, 2009.
[9] W. S. Robertson, M. R. F. Kidner, B. S. Cazzolato, A. C. Zander, "Theoretical design parameters for a quasi-zero stiffness magnetic spring for vibration isolation," Journal of Sound and Vibration, vol. 326, no.1-2, pp. 88–103, 2009.
[10] C. M. Lee, V. N. Goverdovskiy, A. I. Temnikov, "Design of springs with negative stiffness to improve vehicle driver vibration isolation," Journal of Sound and Vibration, vol. 302, pp. 865–874, 2007.
[11] N. Zhou, K. Liu, "A tunable high-static-low-dynamic stiffness vibration isolator," Journal of Sound and Vibration, vol. 329, pp. 1254–1273, 2010.
[12] R. A. Ibrahim, "Recent advances in nonlinear passive vibration isolators," Journal of Sound and Vibration, vol. 314, no. 3–5, pp. 371–452, 2008.
[13] T. D. Le, K.K. Ahn, "Experimental investigation of a vibration isolation system using negative stiffness structure," International Journal of Mechanical Sciences, vol. 70, pp. 99–112, 2013.
[14] K. R. Kim, Y. H. You, H. J. Ahn, "Optimal design of a QZS isolator using flexures for a wide range of payload," International Journal of Precision Engineering and Manufacturing, vol. 14, no. 6, pp. 911–917, 2013.
[15] L. S. Meng, J. G. Sun, W. J. Wu, "Theoretical design and characteristics analysis of a quasi-zero stiffness isolator using a disk spring as negative stiffness element," Shock and Vibration, 2015.

[16] T. P. Dao, S. C. Huang, "Robust design for a flexible bearing with 1-DOF translation using the Taguchi method and the utility concept," Journal of Mechanical Science and Technology, vol. 29, no. 8, pp. 3309–3320, 2015.
[17] T. P. Dao, S. C. Huang, "An optimal study of a gripper compliant mechanism based on Fuzzy-Taguchi method," Applied Mechanics and Material, vol. 418, pp. 141–144, 2013.
[18] T. P. Dao, S. C. Huang, "Design and analysis of a 2-DOF compliant mechanism for nano scale positioning," International Journal of Innovation and Applied Studies, vol. 10, no. 1, pp. 226–236, 2015.
[19] T. P. Dao, S. C. Huang, "Optimization of multiresponse performance measure in slider-rocker compliant mechanism using Fuzzy-Taguchi method," Advanced Materials Research, vol. 683, pp 708–711, 2013.
[20] T. P. Dao, S. C. Huang, "Design and analysis of flexible slider crank mechanism," World Academy of Science, Engineering and Technology International Journal of Mechanical, Aerospace, Industrial, Mechatronic and Manufacturing Engineering, vol. 8, no.5, pp. 784–791, 2014.
[21] T. P. Dao, S. C. Huang, "A flexible bearing with 1-DOF translation for high-precision mechanism,"" Applied Mechanics and Materials, vols. 764-765, pp 155–159, 2015.
[22] T. P. Dao, S. C. Huang, "Optimization of flapper compliant mechanism using fuzzy logic combined Taguchi method," Applied Mechanics and Materials, vol. 300, pp. 710–713, 2013.
[23] T. P. Dao, S. C. Huang, "Design, fabrication, and predictive model of a 1-dof translational, flexible bearing for high precision mechanism," Transactions of The Canadian Society for Mechanical Engineering, vol. 39, no. 3, pp. 419–429, 2015.
[24] T. P. Dao, S. C. Huang, "Design and analysis of compliant rotary joint," Applied Mechanics and Materials, vol. 372, pp. 467–470, 2013.

Thanh-Phong Dao is a researcher at the Institute for Computational Science, Ton Duc Thang University, Ho Chi Minh, Vietnam. He received his Bachelor's Degree in Mechanical Engineering from the Ho Chi Minh City University of Technology and Education, Vietnam in 2008. He received his Master's Degree and Ph. D in Mechanical Engineering from the National Kaohsiung University of Applied Sciences, Taiwan, ROC, in 2011 and 2015, respectively. His interests include compliant mechanism, smart structure, and multi-objective optimization, hybrid optimization algorithms.

Shyh-Chour Huang is a Professor at National Kaohsiung University of Applied Sciences. He received his Bachelor's Degree in Aeronautics and Astronautics Engineering from the National Cheng-Kung University in 1980, Taiwan, ROC. He received his PhD in Mechanical Engineering from the University of Cincinnati, USA in 1990. His research interests include micro-electro-mechanical systems design, biomechanics and multibody dynamics.